Membrane Protein Detection and Morphological Analysis of Red Blood Cells in Hereditary Spherocytosis by Confocal Laser Scanning Microscopy

Laura Rey-Barroso, Mónica Roldán, Francisco J Burgos-Fernández, Ignacio Isola, Anna Ruiz Llobet, Susanna Gassiot, Edurne Sarrate, Meritxell Vilaseca

Microscopy and Microanalysis, 2023, **00**, 1–9
https://doi.org/10.1093/micmic/ozac055

Original Article

Microscopy AND Microanalysis

Membrane Protein Detection and Morphological Analysis of Red Blood Cells in Hereditary Spherocytosis by Confocal Laser Scanning Microscopy

Laura Rey-Barroso[1,*], Mónica Roldán[2,3], Francisco J. Burgos-Fernández[1], Ignacio Isola[3,4], Anna Ruiz Llobet[3,5,6], Susanna Gassiot[3,4], Edurne Sarrate[4,6], and Meritxell Vilaseca[1]

[1] *Centre for Sensors, Instruments and Systems Development, Technical University of Catalonia, Terrassa, Barcelona 08222, Spain*
[2] *Confocal Microscopy and Cellular Imaging Unit, Genetic and Molecular Medicine Department, Pediatric Institute for Rare Diseases, Hospital Sant Joan de Déu, Esplugues de Llobregat, Barcelona 08950, Spain*
[3] *Institute of Pediatric Research, Hospital Sant Joan de Déu, Esplugues de Llobregat, Barcelona 08950, Spain*
[4] *Laboratory of Hematology, Service of Laboratory Diagnosis, Hospital Sant Joan de Déu, Esplugues de Llobregat, Barcelona 08950, Spain*
[5] *Service of Pediatric Hematology, Hospital Sant Joan de Déu, Esplugues de Llobregat, Barcelona 08950, Spain*
[6] *National Institute of Biomedical Research for Rare Diseases, Carlos III Health Institute, Madrid 28029, Spain*

***Corresponding author:** Laura Rey-Barroso, E-mail: laura.rey.barroso@upc.edu

Abstract

In hereditary spherocytosis (HS), genetic mutations in the cell membrane and cytoskeleton proteins cause structural defects in red blood cells (RBCs). As a result, cells are rigid and misshapen, usually with a characteristic spherical form (spherocytes), too stiff to circulate through microcirculation regions, so they are prone to undergo hemolysis and phagocytosis by splenic macrophages. Mild to severe anemia arises in HS, and other derived symptoms like splenomegaly, jaundice, and cholelithiasis. Although abnormally shaped RBCs can be identified under conventional light microscopy, HS diagnosis relies on several clinical factors and sometimes on the results of complex molecular testing. It is specially challenging when other causes of anemia coexist or after recent blood transfusions. We propose two different approaches to characterize RBCs in HS: (i) an immunofluorescence assay targeting protein band 3, which is affected in most HS cases and (ii) a three-dimensional morphology assay, with living cells, staining the membrane with fluorescent dyes. Confocal laser scanning microscopy (CLSM) was used to carry out both assays, and in order to complement the latter, a software was developed for the automated detection of spherocytes in blood samples. CLSM allowed the precise and unambiguous assessment of cell shape and protein expression.

Key words: automated detection, band 3, confocal microscopy, hereditary spherocytosis, immunofluorescence, *in-vivo* imaging, red blood cells, spherical Hough transform

Introduction

Hereditary spherocytosis (HS) is caused by mutations in genes that encode red blood cells (RBCs) membrane proteins (Eber & Lux,2004) involved in vertical associations that link the inner membrane cytoskeleton to the outer lipid bilayer. These proteins transport molecules in and out of cells, attach to other proteins and, in general, maintain cell structure. Among all of them, the band 3 protein plays a central role in the control of cell morphology and deformability, since it is the most abundant protein, and the main component of the Ankyrin and Junctional macromolecular complexes. If there is a defective or lower expression of these proteins, the elastic deformability of RBCs is impaired, they undergo microvesiculation-associated membrane loss and adopt an spherocytic appearance. These spherical RBCs are too stiff to circulate through capillaries, so they are hemolyzed in the microcirculation and phagocytized in the spleen. This causes patients to suffer from different degrees of anemia and other signs and symptoms. Based on the severity of anemia and markers of hemolysis (reticulocyte count and bilirubin), HS can be classified into four forms (Bolton-Maggs et al.,2004). Patients with mild HS (20–30%) are either asymptomatic or present with mild anemia. Moderate HS (60–70%) is usually diagnosed during childhood and causes anemia, jaundice, splenomegaly, and sometimes cholelithiasis, due to elevation in serum bilirubin levels. The moderate/severe form of HS (10%) presents with all the aforementioned symptoms and a more severe anemia. The severe form (3–5%) is characterized by life-threatening anemia and the requirement of frequent blood transfusions, suffering also from splenomegaly, jaundice, and a high risk of developing gallstones. The most affected individuals may have short stature, delayed sexual development, and skeletal abnormalities (Mariani et al.,2008).

The diagnosis of HS is usually based upon clinical manifestations and the parental medical history. HS is inherited in an autosomal dominant pattern for 75% of cases, so one usual criterion for diagnosing a child is that one of the progenitors is also affected by HS. However, this is not always the case, as some mutations are *de novo* or the family history is not available. Initial testing in individuals with suspected HS includes blood smear review and hemolysis testing. Blood smear review under conventional optical microscopy must be performed to assess the presence of spherocytes, which have a

Received: September 2, 2022. **Accepted:** December 20, 2022

round shape and darker color due to the greater amount of hemoglobin on a smaller cell volume, in addition to other abnormal RBC shapes. The percentage of spherocytes is variable. All patients with suspected HS should have a complete blood count with reticulocyte count and RBC indices. The mean corpuscular hemoglobin concentration (MCHC) is often the most useful parameter (an MCHC ≥36 g/dL is compatible with the presence of spherocytes) as well as a low medium corpuscular volume (MCV), especially in neonates. Testing for hemolysis is also necessary and includes lactate dehydrogenase (LDH), indirect bilirubin, haptoglobin, and reticulocyte count. Finally, Coombs testing is usually done to rule out the possibility of immune-mediated hemolysis.

A number of tests are available for confirming the diagnosis of HS. Confirmatory testing can be done in all suspected cases, although some experts may omit them in cases of resource limited settings or in the presence of classic clinical findings in an individual with a confirmed family history of HS. Confirmatory tests include the eosin-5-maleimide (EMA) binding test, osmotic fragility, and osmotic gradient ektacyometry. EMA binds to plasma membrane proteins of RBCs, mainly to band 3 protein. Its expression decreases both in deficiencies of band 3 protein and in other proteins such as ankyrin or spectrin. Under flow cytometry, the mean fluorescence of EMA-stained RBCs in HS patients is lower when compared with control RBCs. In atypical cases, in transfusion dependent patients or if the diagnosis needs to be confirmed with certainty prior to therapeutic splenectomy, DNA studies can be performed, usually involving next generation sequencing (NGS) technology, i.e. custom targeting panels or whole exome sequencing (de Oliveira & Saldanha,2010).

Apart from the inherent limitations of next generation genetic technology (costs, time-consumption, limited availability), approximately 30–50% of patients with hereditary anemias will remain undiagnosed after NGS testing (Russo et al.,2020). This partly arises because of incomplete phenotyping of patients, as supported by the high number of variants of unknown significance of the involved genes (Trujillano et al.,2017). Other limitations are the inability to detect remote intronic mutations, regulatory sequence mutations, and large-scale deletion mutations. This has induced authors in the state of the art to conduct experimental assays to analyze RBCs and improve their phenotypic characterization. Currently, confocal laser scanning microscopy (CLSM) and the fluorescent labeling of the altered membrane proteins is being used to characterize protein expression and morphological traits of RBCs. Complexes CD44 and CD47, for example, have been targeted with the use of different antibodies to reveal differences in fluorescence distribution in normal and congenital dyserythropoietic anemia type II (CDAII) RBCs (Singleton et al.,2018). Band 3 has also been targeted with an antibody (Ab) against its N-terminal and two pharmacological agents. The first produced a loss of affinity at the ankyrin-binding sites, the second produced conformational changes of the cytoplasmic domain. Only the first produced a distinct effect on RBC morphology, while both produced membrane organization changes at the molecular level (Cluitmans et al.,2016). Protein 4.2 has been targeted as well. It binds to band 3, at its N-terminal cytosolic domain. Although both proteins are closely related, certain mutations at their binding site only produce a lower expression of protein 4.2 while maintaining a normal amount of band 3. Full-length wild-type band 3 and mutants associated with HS have been co-expressed with protein 4.2 and were shown to be present at the same level at the membrane using immunofluorescence and confocal microscopy (Bustos & Reithmeier,2011).

Sometimes what is most important is to assess cell morphology rather than fluorescence distribution of certain proteins. It has been proven that in order to perfectly preserve cell shape of RBCs cells must be observed *in vivo* rather than fixated (Khairy et al.,2008; Rappaz et al.,2019). Some works in the state of the art involve the staining of the plasma membrane uniformly with lipophilic dyes that are not protein-specific, solely for the assessment of cellular shape. Fluorescent color dyes Calcein and Vybrant Dil have been used to label the cytoplasm and plasma membrane, respectively, and analyze the three-dimensional (3D) morphology of RBCs. RBCs from a healthy subject have been chemically induced to acquire the characteristic shapes from different pathologies, including spherocytosis. By means of mathematical simulations, authors were able to relate each shape with the amount of shear energy in the membrane-associated cytoskeleton (Khairy et al.,2008). In another work, morphological parameters such as the mean cell volume were obtained and compared for different imaging techniques. Among all of them, CLSM was the one that retrieved the most accurate results; in this case, cells were labeled with the fluorescent dye Vybrant Dil (Rappaz et al.,2019).

In this context, and following our previous study in thalassemia evaluation (Rey-Barroso et al.,2020) we have conducted two experimental assays to characterize RBCs in HS by means of CLSM: an immunostaining assay targeting band 3 to observe its expression in the cell membrane, and a 3D morphological assay with dyes with affinity for the cell membrane and nucleus, to observe shape in living cells and the posterior automated detection of cell shapes and types. This was achieved by the adaptation of a spherical Hough transform algorithm, based in Matlab (The MathWorks Inc., Natick, USA), that is able to automatically detect spherical shapes in 3D volumes; it is also able to distinguish different cell types, like leucocytes, which have a stained nucleus. These two studies are complementary, since sometimes, there is a lower expression of band 3 in the membrane but not necessarily a change in shape of RBCs into spherocytes, and vice versa. The goal is to relate the clinical manifestations of the disease and its severity with the results of these two studies. Unlike other related works, it is possible to preserve the cell shape in perfect conditions by means of the 3D morphological assay since it is carried out *in vivo*. With the algorithm for automatic detection of spherical shapes, we aimed to quantify the number of cells with morphological alterations and relate this parameter to the patients' clinical manifestations and the alterations in band 3 fluorescence.

Materials and Methods

Subjects

Whole blood with tripotassium ethylenediaminetetraacetic acid (EDTA K3) as anticoagulant agent was collected from six pediatric patients, three males and three females between 1 and 18 years old, including patients with different forms of HS and also one healthy child as control. The sample of one progenitor with HS was also collected. The aforementioned assays were conducted in parallel in all samples. The first study sought to reveal variations in the Ab fluorescence intensity along the membrane; the second sought to label the membrane uniformly on fresh samples to be able to preserve the

Table 1. Subjects HS_{1-5}, HS_{P1} and HS_{C1} Laboratory Parameters and Severity.

Patient	Hb (g/dL)	MCV (fL)	MCHC (pg)	%RETI	%HPR	%MICRO	Bilirubin (μmol/L)	HS Severity
HS_1	13.0	70.8	36.8	1.96	6.5	13.5	0.4	Mild
HS_{P1}	13.4	93.0	37.0	6.12	22.9	0.5	2.5	Mild
HS_2	13.6	77.0	36.2	3.13	13.9	5.7	0.9	Mild
HS_3	16.9	86.0	34.9	2.60	5.3	0.9	1.3	Mild
HS_4	14.5	80.0	35.9	3.61	5.6	2.2	0.6	Mild – SPL
HS_5	11.4	88.0	34.9	9.03	9.2	2.0	1.7	Moderate
HS_{C1}	14.5	90.0	33.9	1.70	0.4	0.3	—	—

Hb, hemoglobin in grams per deciliter (g/dL); MCV, medium corpuscular volume in femtoliters (fL); MCHC, medium corpuscular hemoglobin in picograms (pg); %RETI, percentage (%) of reticulocytes; %HPR, percentage of hyperchromic RBCs, %MICRO: percentage of microcytic RBCs.

morphology of RBCs for its analysis. RBC indices for each sample were obtained using an ADVIA 2120i haematology analyzer (Siemens Healthcare Diagnostics Inc., Erlangen, Germany) within 2 h after blood collection Table 1. Pediatric patients with HS are labeled as HS_{1-5}, the progenitor that was also included in the study is HS_{P1}. The healthy child used as a control subject is labeled as HS_{C1}. Subject HS_4 suffered from a severe form of HS and had to be splenectomized (SPL) to improve the hemolytic anemia.

The degree of HS severity for every patient was determined in regards to the manifested clinic and the family medical history, if available. First, the presence of spherocytes on the blood smear was confirmed by inspection under microscopy. Second, a complete blood count was obtained from which the most important RBC indices were considered to be MCHC (pg) >33 and MCV(fL) <80. In addition, %HPR, which is related to the number of spherocytes in the samples, was used as an indicator to confirm what was found in the blood smear previously. Principal indicators of hemolysis were retrieved as well, considering subjects to have a mild form when having Hb (g/dL) ranging from 11 to 15; reticulocyte count (%) from 3 to 6 and bilirubin in micromoles per liter (μmol/L) from 17 to 34. Subjects were considered to have a moderate form when Hb (g/dL) ranges from 8 to 12; reticulocyte count (%) >6 and bilirubin (μmol/L) >34. A subject was considered as severe HS when Hb (g/dL) <8, reticulocyte count (%) >10, and bilirubin (μmol/L) >51.

For the patients with a much equivocal diagnosis yet, HS_4 and HS_5, further NGS testing was carried out. Nevertheless, this genetic studies did not reveal any differences over known mutation places. This study was carried out in accordance with recommendations and protocol approval of the Fundació Sant Joan de Déu Ethics Committee. Written informed consent was obtained from patients and/or their parents or guardians in accordance with the Declaration of Helsinki tenets of 1975 (revised in Tokyo in 2004).

Sample Preparation

Immunofluorescence Assay

For the immunostaining assay, band 3 was the target protein to label. As mentioned above, whole blood with EDTA K3 was used to avoid the formation of clots. Cells were fixed with paraformaldehyde 2%, and then blocked with PBS-BSA 1%. Afterwards, they were incubated with BRIC 200, a primary monoclonal mouse Ab, which is specific for biding the extracellular domain of band 3 on the extracellular loop between amino acids 545 and 567; it is also known to agglutinate normal RBCs indirectly. The fluorochrome molecule attached to the Ab was iFluor488 (International Blood Group Reference Laboratory, Bristol, UK). Finally, samples were mounted over slides with cover slips to acquire 3D stacks of the fluorescence distribution of the Ab over the membrane.

Morphology Assay

For the *in-vivo* study of the RBCs morphology, whole blood freshly extracted without the addition of solvents or any other kind of saline solution was used. Only the addition of EDTA K3 in the extraction tubes as anticoagulant agent was included. Samples were loaded into cell culture dishes CELLview ™ (Greiner Bio One GmbH, Courtaboeuf, France), which incorporate a cell-adhesion layer that prevents cellular movement when capturing an image stack. The cell membrane was stained with CellMask ™ Deep Red (Thermo Fisher Scientific Inc., Waltham, USA). The nuclei of leucocytes were stained with Hoechst 33342 (Thermo Fisher Scientific Inc., Waltham, USA), in order to distinguish them from RBCs. Temperature and CO_2 control inside the microscope were enabled for the best sample preservation. The 3D stacks of the samples were acquired to evaluate cell morphology and the number of spherocytes present in the samples.

Image Acquisition

The samples were analyzed under a Leica TCS SP8 confocal microscope equipped with a white light laser and resonant scanner module (Leica Microsystems GmbH, Mannheim, Germany). It incorporates hybrid detectors capable of detecting signals with high sensitivity coming from RBCs from 400 to 790 nm. The microscope has three lasers for excitation: a diode laser with an excitation of 405 nm, argon laser with an excitation in blue at 488 nm, and a white laser that excites from 470 to 670 nm, combined with an acoustic-optic tuneable filter (AOTF). Microscope settings and acquisition sequences used on every assay are detailed below. Images of both assays were generated using the Leica LAS X software (Leica Microsystems GmbH, Mannheim, Germany).

Immunofluorescence Assay

For the case of the immunostained cells, emission was collected with a 40× (NA 1.1, water) plan-apochromatic objective and a 1.5 airy unit (AU) pinhole. BRIC 200, whose fluorescent probe was iFluor488, was excited with the argon laser and AOTF set at 488 nm and 20% power and 510–560 nm detection window. An image acquisition sequence *xyz* to acquire eight axial sections (step size = 1 μm) of the fluorescence distribution of the band 3 protein along cell

thickness was performed. A galvanometric unidirectional speed of 600 Hz was applied to the emission detection. The image format chosen was 12-bit and 1024 × 1024 pixels resolution. Between 5 and 10 fields were acquired for each sample with a field of view (FOV) of approximately 166 × 166 μm. Appropriate negative controls were used to adjust confocal settings and avoid nonspecific fluorescence artifacts. To compare the confocal data, identical confocal settings were used for image acquisition in different samples.

3D Morphology Assay

For the case of the assessment of cell shape *in-vivo*, Hoechst 33342 DNA label was excited with a blue diode laser (405 nm) and detected in the 415–470 nm range. The CellMask™ dye was excited with a white laser and AOTF set at 633 nm, 70% power, and detected in the 650–795 nm range; the objective used was a 63× (NA 1.40, oil) plan-apochromatic with a 1 AU pinhole. An image acquisition sequence *xyz* for both channels was used to acquire the 3D stacks of the fluorescence distribution of the two fluorescent color dyes. Emission detection was performed at a galvanometric bidirectional speed of 8000 Hz, looking for a tradeoff between avoiding cell movement artifacts and providing sufficient exposure time for excitation. The image format chosen was 8-bit, 800 × 800 pixels resolution; 45 sections (step size = 0.299 μm) were acquired to get an image volume stack of 13.5 μm in total thickness. Finally, images were deconvoluted using the software Huygens Professional Software v17.10.0p8 (Scientific Volume Imaging B.V., Leiden, The Netherlands) in order to improve image quality. For each sample, 5–10 fields of approximately 52.8 × 52.8 μm FOV were acquired, each one including a complete volume stack.

Image Processing

Immunofluorescence Assay

The image processing software Fiji (National Institutes of Health, Bethesda, USA) was used to visualize Ab BRIC 200 fluorescence distribution, which targets band 3, and obtain the sum projection of the images 1–8 of each stack, from which the mean fluorescence of the samples could be retrieved. In addition, an image processing protocol of thresholding, illustrated in Figure 1, was applied to the central image of every stack, to quantify cell population. Mean fluorescence was then divided by the total number of cells. The automated cell-counting algorithm is original and it was the result of applying different thresholding algorithms and image processing steps. First, the image is converted to 8-bit unsigned, and inverted. Next, a Niblack local threshold (Niblack,1986) with local domain radius set to 15 is applied, and the noise in the form of dark outliers is removed from the subsequent images. Then, a closing operation is applied plus one or two steps of dilation, if needed. Finally, the automatic search for maxima over the image provided by Fiji's processing toolbox easily retrieves a central point on every cell. Manual cell counting with Fiji's labeling tool was also carried out to check the accuracy of the algorithm.

3D Morphology Assay

The visualization of the high-quality 3D image stacks was carried out with Leica LAS X software. CellMask™ dye was evenly distributed over cell membranes with a bright, deep red color that permitted the precise assessment of morphology by visual inspection. A typical RBC is normocytic, has a biconcave shape with a diameter of 7.5 μm, and it is normochromic, with an area of central pallor equal to approximately 30–45%

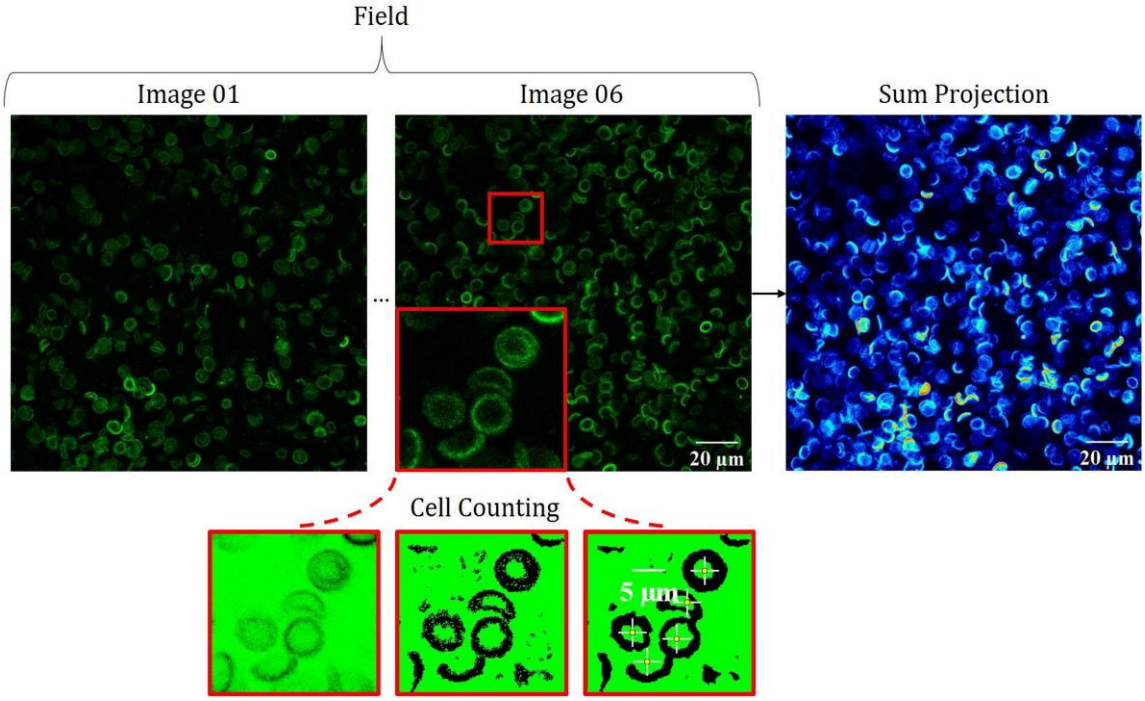

Fig. 1. Top: fluorescence images 01 and 06 of an image stack (field) and sum projection of images. Bottom: detail of image 06 and resulting images from the image processing algorithm for cell counting: image inversion (left), application of local threshold and elimination of dark outliers (center), and closing operation and application of function *Find Maxima* of Fiji software (right).

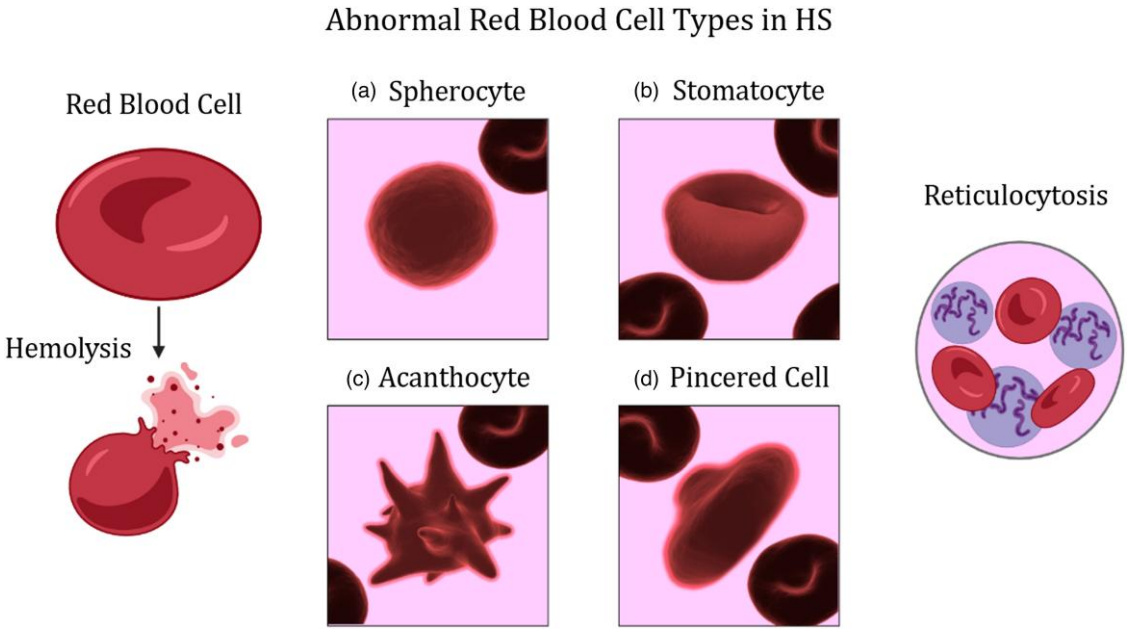

Fig. 2. Left: A normal biconcave RBC and how defects in the membrane proteins result in RBCs' hemolysis. Center: Abnormal RBC types that may appear in HS: (**a**) a spherocyte, the predominant form, (**b**) a stomatocyte, (**c**) an acanthocyte, and (**d**) a pincered cell. Right: Reticulocytosis in the blood stream, which is a result to counteract hemolysis by increasing RBC precursors.

Table 2. User-defined Parameters and Selected Values for the Spherical Hough Transform.

Parameter	Value	Units	Description
Object radius	30–40	pixels	Radius of spheres to be located, equivalent to spherocytes radius range
Gradient threshold	0.24	—	Intensity gradient threshold used to eliminate uniform areas before the voting process
Filter radius	35	pixels	The radius of the filter used for the search of local maxima in the accumulation array
Multiple radius tolerance	1	—	Ability to detect concentric spheres (0) or just simple spheres (1)
Object center intensity	0	—	Keeps only the detected objects with the indicated center intensity and above

of the diameter. Spherocytes are the predominant morphologic abnormality in patients with HS, they are microcytic (smaller than normal) cells with a spherical shape and lacking a central pallor. They are hyperchromic due to the highest concentration of hemoglobin on a smaller volume due to the loss of membrane surface area. Less commonly, small, dense spherocytes, and bizarre RBC morphology with anisocytosis and poikilocytosis may arise. Certain morphological findings are associated with defects in certain membrane proteins such as pincered cells with band 3, acanthocytes with β spectrin, or stomatocytes with protein 4.2 (Gallagher,2013). These are illustrated in Figure 2, but primarily spherocytes were found, and the amount of spherocytes was different from one sample to another.

The automated detection of spherocytes was carried out with the adaptation of the Matlab-based spherical Hough transform software in the MATLAB Central File Exchange repository (Xie,2022). Matlab version used was R2021b with an NVIDIA graphics card model Quadro RTX 8000 (NVIDIA Corp., Santa Clara, USA) for the computation of the algorithm. The 3D Hough transform is an edge detection algorithm. Curves are plotted through every point in the surface of a given 3D shape, in this case, a sphere (infinite curves). The curve that happens to go across more points in the isosurface of the sphere gets a higher number of votes in a so-called accumulator space, explicitly constructed by the algorithm

$$(i-a)^2 + (j-b)^2 + (k-c)^2 = r^2. \quad (1)$$

Equation (1) is the general equation for a sphere in the 3D space with a certain radius. At first, all the possible spheres that can be represented in the 3D space are possible options that could go across the edge of an actual spherocyte, and will undergo a voting process. The accumulator space is made up of one cell for each pixel in the 3D space image, i.e. the space where spheres are going to be detected, and each cell is initially set to 0. For each edge point (i, j, k) of a sphere (in this case, spherocyte), there is an increment in all cells (voting) which, according to equation (1), could be the center of a sphere. Then, the local maxima in the cells of the accumulator space represent spheres that were actually detected by the algorithm. Modern algorithms also consider the intensity gradient of the image, therefore significantly reducing the amount of computations in the voting procedure.

The algorithm was able to detect microcytic and hyperchromic spherocytes. A series of preset parameters had to be carefully adjusted for the optimal detection of spherocytes in the heterogeneous set of samples and the reduction of computationally expensive operations. Most importantly, the radius of spherocytes that were trying to be located was set to 30–40 pixels. Voxel size is $0.0660 \times 0.0660 \times 0.2985\,\mu m^3$, therefore, the volume of a spherocyte is approximately 70–80 μm^3 (or fL), which is in accordance to the MCV data of our subjects in Table 1. The diameter in pixels of the spherocytes was measured with Matlab's Image Viewer application

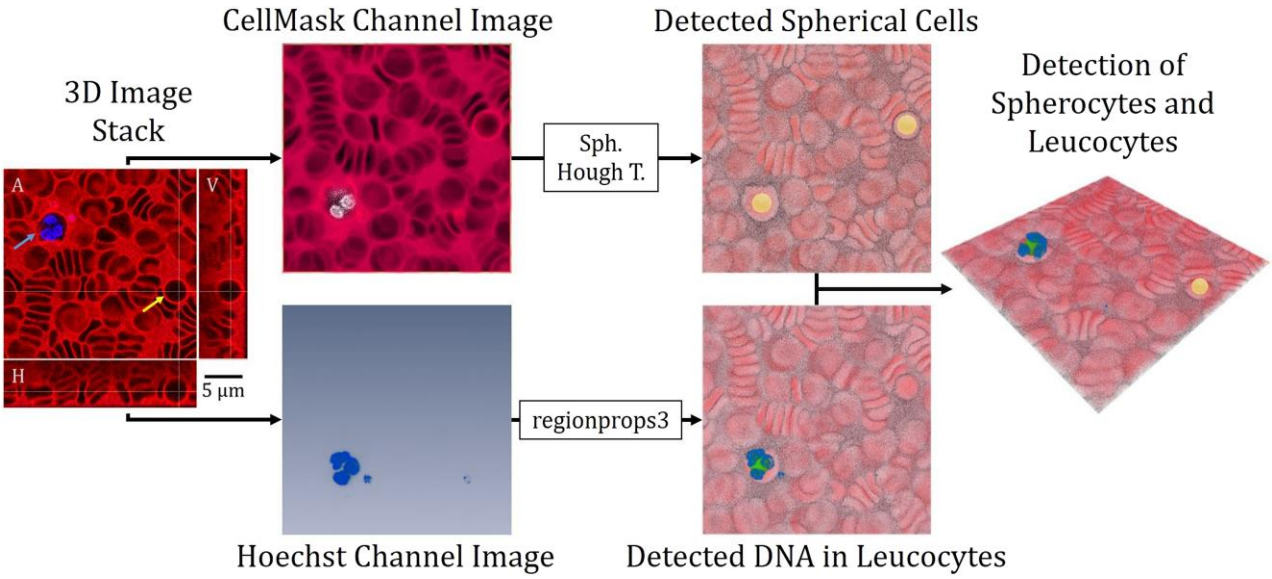

Fig. 3. Process for the algorithm to detect spherocytes and leucocytes. From left to right: Original 3D image stack, where the position of a leucocyte (blue arrow) and the position of a spherocyte (yellow arrow) are indicated. It is split into two image channels, the one containing the information of the stained membranes with CellMask is made isometric and inverted, then the spherical Hough transform is applied to it and all spherical cells are detected (yellow spheres). At the same time, the image channel containing the stained nuclei has function regionprops3 applied to it, and all leucocytes' nuclei are detected as well (green spheres). Finally, both images are compared by the algorithm and the final positions of leucotytes and spherocytes are determined, in the last image where the position of a spherocyte (yellow sphere) and the position of the blue DNA mass inside the leucocyte (green sphere) are indicated.

(Image Processing Toolbox 10.4). In addition, this algorithm takes into account the gradient field of intensities in the image and removes pixels with gradient magnitudes smaller than a certain threshold from the voting process. This threshold was set to 0.24 to remove the parts of the image with uniform intensity from the computation. These and other secondary parameters that were experimentally identified are detailed in Table 2.

On top of each detected spherocyte, the algorithm plots a sphere with a radius of 35 pixels. Then, in order to detect and possibly eliminate, if detected as spherocytes, the presence of leucocytes, which are bigger, spherical, and nucleated cells, the information of the second channel in the 3D image stacks was used; this second channel contained the emission of the nuclei stained in blue by Hoechst 33342. With Matlab's function regionprops3 the centroids and diameters of the masses of stained genetic material were retrieved; only masses of labeled DNA with a diameter greater than 30 pixels were considered to be nuclei. A sphere of 35 pixels of diameter, which is the size of the spheres located at the detected spherocytes, is then plotted in the centroid coordinates for each mass. Finally, their centroid coordinates are compared to those of the detected spherocytes, and if any are laying within a distance of 30 pixels above or below for every direction in space, that centroid point is eliminated from the image representing detected spherocytes. The effectiveness of the adapted spherical Hough transform algorithm is illustrated in Figure 3.

Results and Discussion

Immunofluorescence Assay

Figure 4 shows the mean fluorescence signal normalized by the computed number of RBCs for each patient. Mean fluorescence of BRIC 200 is visibly higher for the control than for the HS subjects; this may provide a hint about the lack of

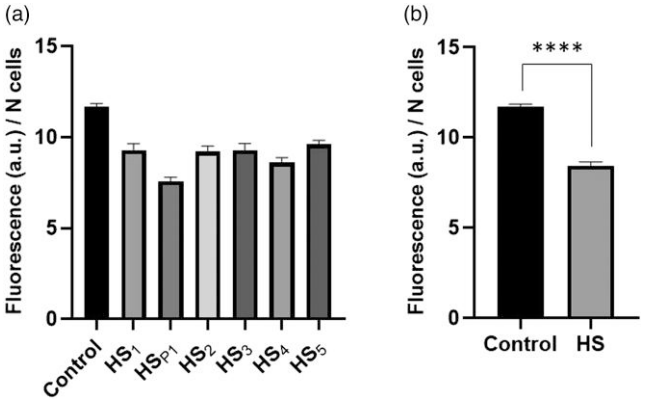

Fig. 4. (**a**) Mean fluorescence (in a.u.) divided by the cell population (N cells) for each of the subjects. (**b**) Mean fluorescence of the control compared to the averaged mean fluorescence of all HS subjects. Data were analyzed by the Wilcoxon-paired test (****$p < 0.0001$).

expression of the protein band 3 in HS as it is suggested in other related works (Cluitmans et al.,2016). In addition, this is in accordance to the results that hematologists obtain from an EMA binding test. Contrary to what is described in other works, we did not appreciate differences in how the Ab is distributed in the membrane. This is probably due to the high cell density of our samples or the indirect hemagglutination produced by the Ab. In addition, a different image acquisition protocol using STED superesolution could have been useful to retrieve subtle differences in the distribution of band 3 protein in the membrane.

3D Morphology Assay

Healthy RBCs presented the characteristic biconcave shape and central pallor region. Spherocytes could be identified as

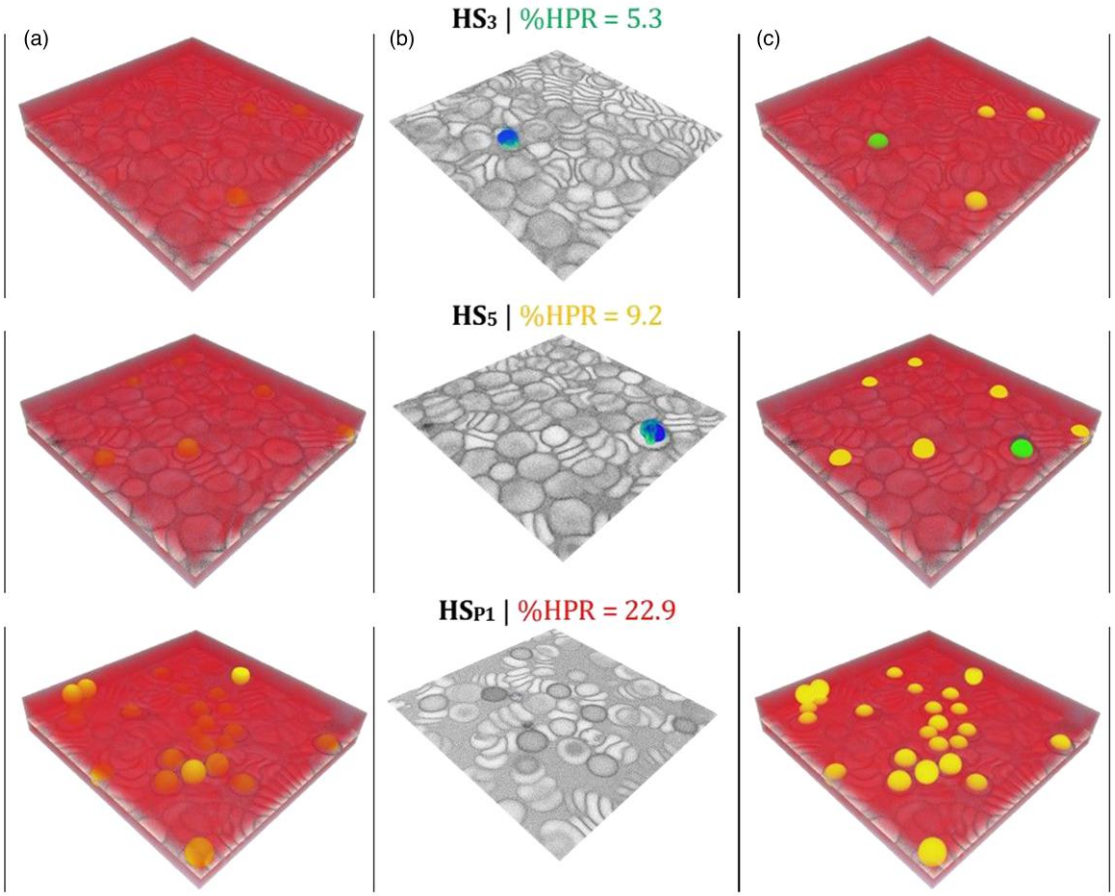

Fig. 5. 3D image stacks for three different subjects: HS_3 with a mild form of HS and %HPR = 5.3; HS_5 with a moderate HS and %HPR = 9.2; and HS_{P1} with a mild HS and %HPR = 22.9. (**a**) 3D image of the CellMask emission with detected spherical forms (yellow spheres), (**b**) 3D image of the Hoechst 33342 emission with detected leucocytes nuclei (blue spheres), (**c**) emission images of CellMask and Hoescht 33342 including detected spherocytes (yellow spheres) and leucocytes (green spheres).

Table 3. Spherical Hough Transform Performance in Terms of Detected Spherocytes and Leucocytes; Other Structures Detected as Spherocytes and Overall Error for Each Subject.

Patient	Total Spherocytes	Detected Spherocytes	Total Leucocytes	Detected Leucocytes	Others Detected	Overall Error (%)
HS_1	0	0	0	0	18	0.00
HS_{P1}	67	48	1	1	23	28.35
HS_2	45	30	1	1	22	33.33
HS_3	5	5	1	1	17	0.00
HS_4	2	2	4	4	34	0.00
HS_5	3	3	2	2	15	0.00
HS_{C1}	0	0	2	3	12	0.00

well, as rounder, smaller, hyperchromic cells. Both were easily distinguished from leucocytes due to their bright blue nuclei stained with Hoechst 33342. Figure 5 presents the 3D image stacks of a field for three different subjects, each with a different %HPR, and how the spherical Hough transform algorithm detected the spherocytes and leucocytes. In Figure 5a, the red emission from the evenly stained cell membranes and the detected spherical forms (yellow spheres) are represented altogether. Figure 5b represents the DNA stained masses inside the nuclei of leucocytes, in blue-green, and the detection that the algorithm performs for those masses that reach 60 pixels in diameter (blue spheres). Figure 5c is the combination of images 5a and 5b.

In Figure 5, only one field per subject is shown for illustrative purposes, but 10 to 12 fields for each subject were acquired in order to have at least four fields available to check on the effectiveness of the algorithm. Considering the high population of cells per field, this number was considered statistically significant. Fields for each subject were analyzed to estimate the total number of spherocytes by means of the spherical Hough transform algorithm. Manual counting through visual inspection was carried out to check the accuracy of the algorithm. In Table 3, the total number of spherocytes and total number of leucocytes (ground truth) were considered to be the ones determined by visual inspection of four fields for every subject. From the manual and automated

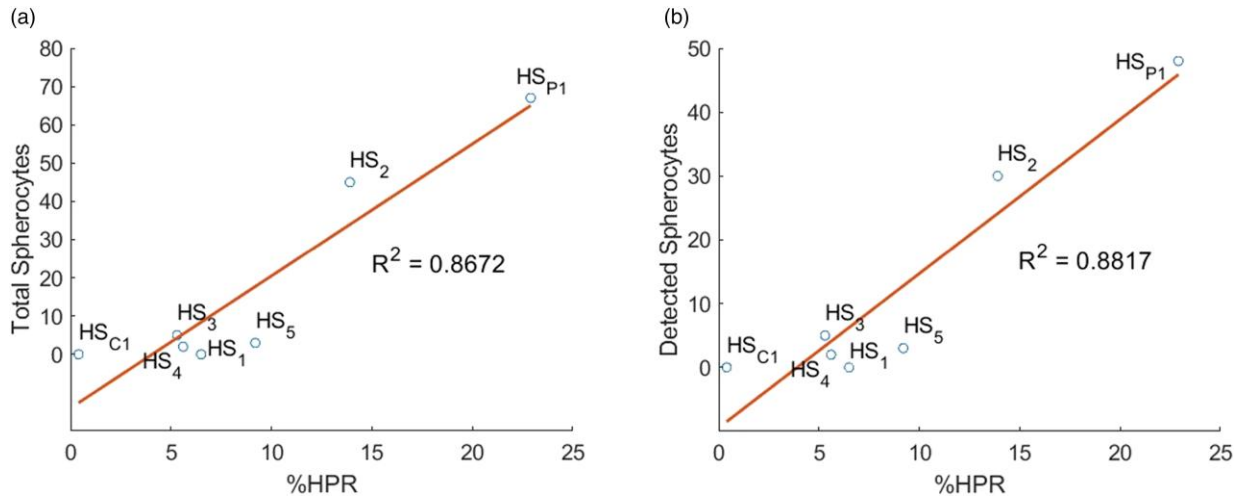

Fig. 6. (**a**) Relation among %HPR and the number of spherocytes determined by visual inspection and (**b**) relation among %HPR and the number of detected spherocytes by means of the Spherical Hough transform algorithm. The R^2 value shows there is a high correlation between %HPR and these two parameters.

cell counts, the accuracy of the algorithm performance on every subject is expressed as the overall error, which is the total number of spherocytes minus the number of spherocytes correctly detected, divided by the total number of spherocytes. Other parts of the samples with spherical shapes that were also detected by the algorithm are included as well.

The algorithm precisely estimates the number of spherocytes in most cases. Nevertheless, in fields were few or no spherocytes are present, the algorithm is prone to detect some other structures as spheres. The detection of leucocytes retrieved almost perfect results. As expected, there is a relationship between %HPR and the number of spherocytes present on each sample (Fig. 6). %HPR has been reported by some as a useful screening tool for patients with HS (Rooney et al.,2020).

Conclusions

The use of CLSM for the analysis of RBC in HS patients has proven its potential for the evaluation of different cellular components, and in this case, it has made possible the identification of a band 3 deficiency in the HS patients. Unlike conventional microscopy, CLSM allows precise and unambiguous assessment of 3D cell shape. This, in combination with the automated detection of shapes and patterns, will probably allow the identification of this and other pathologies in the near future. In this work, we were able to automatically detect spherocytes successfully, as demonstrated by the correlation between the number of detected spherocytes and the %HPR for every subject. Research efforts are now focused on trying to label other membrane proteins that are known to be affected in HS and find biomarkers to better discriminate between mild and moderate forms of HS. For this purpose, protocols on color labeling and preservation of this kind of samples, which are corrupted in a very short time window, are being investigated.

Financial Support

This publication is part of the project PID2020-112527RB-I00, funded by CIN/AEI/10.13039/501100011033. Laura Rey-Barroso thanks the Ministry of Science, Innovation and Universities for the PhD (FPI) grant she has received (DPI2017-89414-R). The current study has been funded by the Spanish National Agency of Investigation (AEI).

Conflict of Interest

The authors declare that they have no competing interest.

References

Bolton-Maggs PH, Stevens RF, Dodd NJ, Lamont G, Tittensor P & King MJ (2004). Guidelines for the diagnosis and management of hereditary spherocytosis. *Br J Haematol* **126**, 455–474. https://doi.org/10.1111/j.1365-2141.2004.05052.x

Bustos SP & Reithmeier RAF (2011). Protein 4.2 interaction with hereditary spherocytosis mutants of the cytoplasmic domain of human anion exchanger 1. *Biochem J* **433**, 313–322. https://doi.org/10.1042/BJ20101375

Cluitmans JCA, Gevi F, Siciliano A, Matte A, Leal JKF, De Franceschi L, Zolla L, Brock R, Adjobo-Hermans MJW & Bosman GJGCM (2016). Red blood cell homeostasis: Pharmacological interventions to explore biochemical, morphological and mechanical properties. *Front Mol Biosci* **29**, 312–326. https://doi.org/10.3389/fmolb.2016.00010

de Oliveira S & Saldanha C (2010). An overview about erythrocyte membrane. *Clin Hemorheol Microcirc* **44**, 63–74. https://doi.org/10.3233/CH-2010-1253

Eber S & Lux SE (2004). Hereditary spherocytosis: Defects in proteins that connect the membrane skeleton to the lipid bilayer. *Semin Hematol* **41**, 118–141. https://doi.org/10.1053/j.seminhematol.2004.01.002

Gallagher PG (2013). Abnormalities of the erythrocyte membrane. *Pediatr Clin North Am* **60**, 1349–1362. https://doi.org/10.1016/j.pcl.2013.09.001

Khairy K, Foo J-J & Howard J (2008). Shapes of red blood cells: Comparison of 3D confocal images with the bilayer-couple model. *Cell Mol Bioeng* **1**, 173–181. https://doi.org/10.1007/s12195-008-0019-5

Mariani M, Barcellini W, Vercellati C, Marcello AP, Fermo E, Pedotti P, Boschetti C & Zanella A (2008). Clinical and hematologic features of 300 patients affected by hereditary spherocytosis grouped according to the type of the membrane protein defect. *Haematologica* **93**, 1310–1317. https://doi.org/10.3324/haematol.12546

Niblack W (1986). *An Introduction to Digital Image Processing*. Englewood Cliffs, NJ: Prentice-Hall.

Rappaz B, Barbul A, Emery Y, Korenstein R, Depeursinge C, Magistretti PJ & Marquet P (2019). Comparative study of human erythrocytes by digital holographic microscopy, confocal microscopy, and impedance volume analyzer. *Cytometry A* **73**, 895–903. https://doi.org/10.1002/cyto.a.20605

Rey-Barroso L, Roldán M, Burgos-Fernández FJ, Gassiot S, Ruiz Llobet A, Isola I & Vilaseca M (2020). Spectroscopic evaluation of red blood cells of thalassemia patients with confocal microscopy: A pilot study. *Sensors* **20**, 4039. https://doi.org/10.3390/s20144039

Rooney S, Hoffmann JJ, Cormack OM & McMahon C (2020). Screening and confirmation of hereditary spherocytosis in children using a CELL-DYN Sapphire haematology analyser. *Int J Lab Hematol* **37**, 98–104. https://doi.org/10.1111/ijlh.12245

Russo R, Marra R, Rosato BE, Iolascon A & Andolfo I (2020). Genetics and genomics approaches for diagnosis and research into hereditary anemias. *Front Physiol* **11**, 613559. https://doi.org/10.3389/fphys.2020.613559

Singleton BK, Ahmed M, Green A, Heimpel H, Wozniak MJ, Ranjha L, Seeney F, Bomford A, Mehta P, Guest A, Mushens R & King MJ (2018). CD44 as a potential screening marker for preliminary differentiation between congenital dyserythropoietic anemia type II and hereditary spherocytosis. *Clin Cytom* **94**, 312–326. https://doi.org/10.1002/cyto.b.21488

Trujillano D, Bertoli-Avella AM, Köster J & Marais A, *et al.* (2017). Clinical exome sequencing: Results from 2819 samples reflecting 1000 families. *Eur J Hum Genet* **25**, 176–182. https://doi.org/10.1038/ejhg.2016.146

Xie L (2022). Spherical Hough transform for 3D images. *MATLAB Central File Exchange*. Available at https://www.mathworks.com/matlabcentral/fileexchange/48219-spherical-hough-transform-for-3d-images